13th World Conference on Earthquake Engineering
Vancouver, B.C., Canada
August 1-6, 2004
Paper No. 207

THE INFLUENCE OF AMPLITUDE AND PHASE DIFFERENCES IN BI-DIRECTIONAL GROUND MOTION ON THE BEHAVIOUR OF IRREGULAR STRUCTURES.

Nicholas A ALEXANDER[1]

SUMMARY

The generation of an applied torque spectrum for asymmetric building structures is discussed. The critical conditions surrounding peaks in this torque spectrum are noted. They are found to be a function of phase tuning of component frequencies. A parameter termed the degree of phase tuning is proposed. Larger values of the degree of phase tuning produce larger total power of the applied torque. The degree of phase tuning is investigated for actual accelerogram records and found to be different. The influence of this applied torque on the structural response of the building system is investigated. Larger degrees of phase tuning produce larger power of the torsional structural response. The importance of the degree of phase tuning is underlined with reference to selection of a statistically unbiased set of accelerograms selected for nonlinear timehistory analysis of asymmetric structures.

INTRODUCTION

In recent years there has been a move towards nonlinear time-history analysis of building structures subject to seismic actions. This has mainly been due to increased computational power and better more useable nonlinear finite element codes. The feasibility of performing such analyses on complex, materially nonlinear building structures has come into the realm of the engineering designer not just the researcher. Though, perhaps, this is true only for unusual, expensive or safety critical structures at present. The most widely used alternative is, of course, classical linear modal analysis which employs a pseudo-nonlinear and highly smoothed design spectrum. The disadvantages of using modal analysis are well known; however the design spectrum contains a useful summary and, in some crude sense, a probabilistic interpretation of the characteristics of a spectrum of severe seismic events. Thus the abandonment of modal analysis in favor of a nonlinear time-history approach raises the question about how to use the design spectrum. Many researchers have advocated using the design spectrum to generate a series of artificial accelerograms. Typically, the amplitude spectrum of an artificial and "random signal" are adjusted such that the response spectrum of a single degree of freedom system matches approximately the design spectrum. The phase content of the artificial record is typically maintained as random. An alternative is to use recorded accelerograms for actual seismic events. In both cases the question remains about the selection of accelerograms and how many to use for the purposes of a reliable estimate of the performance of the building structure when subject to the unknown future seismic event.

[1] Lecturer in Structural Engineering, Department of Civil Engineering, University of Bristol, UK.

This paper considers the analysis of asymmetric building structures. Particularly it attempts to determine if certain critical phase and amplitude combinations in orthogonal accelerogram pairs can produce more or less torsional motion in such structures. The reason why this may be important is that it is currently typical to use only a small sample of real accelerograms, perhaps only 3, [1], in a nonlinear timehistory analysis. A small sample may or may not accurately describe an unknown population statistic, and often it doesn't; unless more information is known about the characteristics of the unknown population. The unknown population here is the probability of a certain unknown future seismic event producing a particular critical structural response. In the case of artificial accelerograms a larger number of records are often used. However, without understanding of the effect of the ground motion phase components on the structural performance, it is still possible that miss-represent the unknown population statistics.

FREQUENCY COMPONENTS OF APPLIED INERTIAL TORQUE

By a process of sub-structuring that adopts three master degrees of freedom(x, y, θ), a multi-storey building structure can be idealized by the following single storey idealization, shown in Figure 1. The lumped building mass *m* is eccentrically supported by a hypothetical column. The equation of motion, under linearly elastic conditions, of such a structure is well documented [2], [3], etc. ; and it can, in any case, be derived by employing Euler-Lagrangian equations derived from the variational principle of least action. Thus equation of motion, defined with a coordinate origin at the elastic centre of stiffness, is as follows in equation (1)

$$\begin{bmatrix} 1 & 0 & \varepsilon_y \\ 0 & 1 & -\varepsilon_x \\ \varepsilon_y & -\varepsilon_x & 1 \end{bmatrix} \begin{bmatrix} \ddot{x} \\ \ddot{y} \\ r\ddot{\theta} \end{bmatrix} + [C] \begin{bmatrix} \dot{x} \\ \dot{y} \\ r\dot{\theta} \end{bmatrix} + \begin{bmatrix} \omega_x^2 & 0 & 0 \\ 0 & \omega_x^2 & 0 \\ 0 & 0 & \omega_\theta^2 \end{bmatrix} \begin{bmatrix} x \\ y \\ r\theta \end{bmatrix} = - \begin{bmatrix} \ddot{x}_g \\ \ddot{y}_g \\ \varepsilon_y \ddot{x}_g - \varepsilon_x \ddot{y}_g \end{bmatrix} \tag{1}$$

$$[M]\underline{\ddot{u}} + [C]\underline{\dot{u}} + [K]\underline{u} = -\underline{\ddot{u}}_g$$

where *r* is the radius of gyration of the building mass defined at the origin of the building. Eccentricity ratios $\varepsilon_x = e_x / r, \varepsilon_y = e_y / r$ Frequency parameters $\omega_x^2 = K_x / m, \omega_y^2 = K_y / m, \omega_\theta^2 = K_\theta / mr$. $[C]$is a damping matrix. $\ddot{x}_g, \ddot{y}_g$ are the orthogonal, horizontal, ground motion components that excite the structure. The external actions have a torque component $\tau(t)$ which can be obtain for the last row of the RHS of equation (1) hence equation (2)

$$\tau(t) = \ddot{x}_g(t)\varepsilon_y - \ddot{y}_g(t)\varepsilon_x \tag{2}$$

By employing a Fourier transform of $\ddot{x}_g, \ddot{y}_g$, the influence of a frequency component $\mathrm{T}(\omega)$ of the torque $\tau(t)$ is given by equation (3). Now the modulus of this expression is given by equation (5) where the phase difference spectra, equation (4).

$$\ddot{x}_g(t) = \tfrac{1}{2\pi}\int_{-\infty}^{\infty} A_x(\omega)\exp(i\phi_x(\omega))\exp(i\omega t)\, d\omega \ , \ \ddot{y}_g(t) = \tfrac{1}{2\pi}\int_{-\infty}^{\infty} A_y(\omega)\exp(i\phi_y(\omega))\exp(i\omega t)\, d\omega$$

$$\tau(t) = \tfrac{1}{2\pi}\int_{-\infty}^{\infty} \mathrm{T}(\omega)\exp(i\omega t) d\omega$$

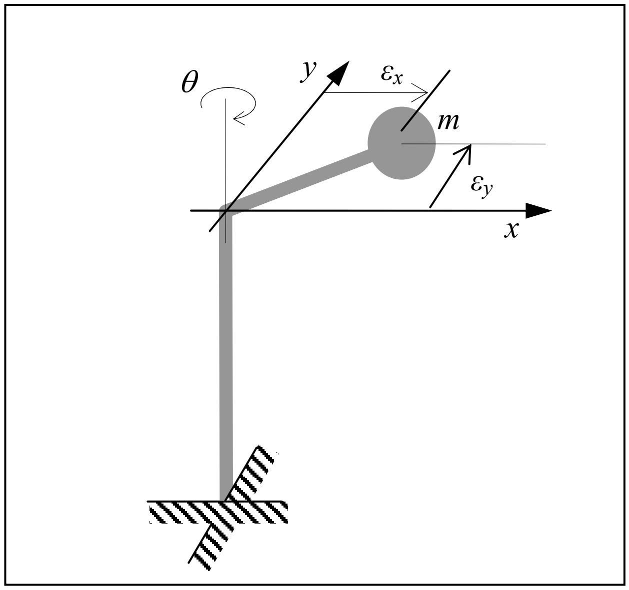

Figure 1, idealized eccentric single storey structure

$$\mathrm{T}(\omega)=\exp(i\phi_x(\omega))\left\{\left(A_x(\omega)\varepsilon_y-A_y(\omega)\varepsilon_x\cos(\phi_D(\omega))\right)-iA_y(\omega)\varepsilon_x\sin(\phi_D(\omega))\right\} \quad (3)$$

$$\phi_D(\omega)=\phi_y(\omega)-\phi_x(\omega) \quad (4)$$

$$|\mathrm{T}(\omega)|^2=\left\{\left(A_x(\omega)\varepsilon_y\right)^2+\left(A_y(\omega)\varepsilon_x\right)^2\right\}-\left\{2\left(A_y(\omega)\varepsilon_x\right)\left(A_x(\omega)\varepsilon_y\right)\cos(\phi_D(\omega))\right\}=\mu(\omega)-\sigma(\omega) \quad (5)$$

Phase tuning

The term $\mu(\omega)$ represents an amplitude dependent term of torque power, i.e. the part that is not affected by *phase tuning.* $\sigma(\omega)$ is an amplitude and phase difference dependent term, of the torque power, i.e. the part that is affected by phase tuning. The terms $\mu(\omega)$ and $\sigma(\omega)$ can only be evaluated numerically for particular accelerogram pairs. In order to provide a meaningful comparison the following accelerograms are scaled using their Arias intensities [4]. The mean Arias intensity I_a of $\ddot{x}_g$ and $\ddot{y}_g$ is compute, equation (6) and then the $\ddot{x}_g, \ddot{y}_g$ accelerograms by dividing by $\sqrt{I_a}$. Thus the normalized, scaled, accelerogram pair has a new mean Arias intensity of 1 m/s. This also implies that, for the condition of equal eccentricity ratios, the total power of the fixed amplitude dependent term $\sigma(\omega)$ in equation (5) is constant, shown in (6), for any normalized accelerogram pair.

$$I_a=\frac{\pi}{2g}\frac{1}{2}\left(\int_{-\infty}^{\infty}\ddot{x}_g(t)^2\,dt+\int_{-\infty}^{\infty}\ddot{y}_g(t)^2\,dt\right) \quad , \quad \int_{-\infty}^{\infty}\mu(\omega)d\omega=\frac{4g\varepsilon_x^2}{\pi} \quad (6)$$

Figure 2, graphically displays equation (5) for a two accelerogram pairs. For this figure the eccentricity ratios are $\varepsilon_x=\varepsilon_y=0.1$. Figure 2 also displays the relative magnitudes of terms $\mu(\omega)$ and $\sigma(\omega)$. It is clear from visual inspection that torque power for the Kobe event is larger that for the Northridge event. Remember the mean total power of $\ddot{x}_g$ and $\ddot{y}_g$ the same for both events, due to scaling. This difference in magnitude is not dependant on scaling, or is it dependant on the structural configuration; though larger eccentricities will generally increase the torque power. The difference is entirely due to the phase tuning term $\sigma(\omega)$. Both graphs are displayed from 0 to 5 Hz as almost all the power is limited to this narrow range. The frequencies at which peaks in the torque power occur are often caused by phase tuning as well as larger amplitudes. In the Northridge example plot the peak at 0.8Hz is amplified by phase tuning in this way. However this is not a universal result. Consider the peak at about 2.4Hz in this plot, the phase difference is such that it has almost no effect torque power. At 2.4Hz there are larger amplitude than at 0.8Hz but the phase tuning is such that they are not utilized because $\sigma(2\pi 2.4) \approx 0$. This is important, for *knowledge of amplitude content is necessary but not sufficient to quantify torque power*. The selection of accelerogram pairs for time-history analysis based solely on total power such as Arias intensities etc. will miss some important information in the case of asymmetric buildings.

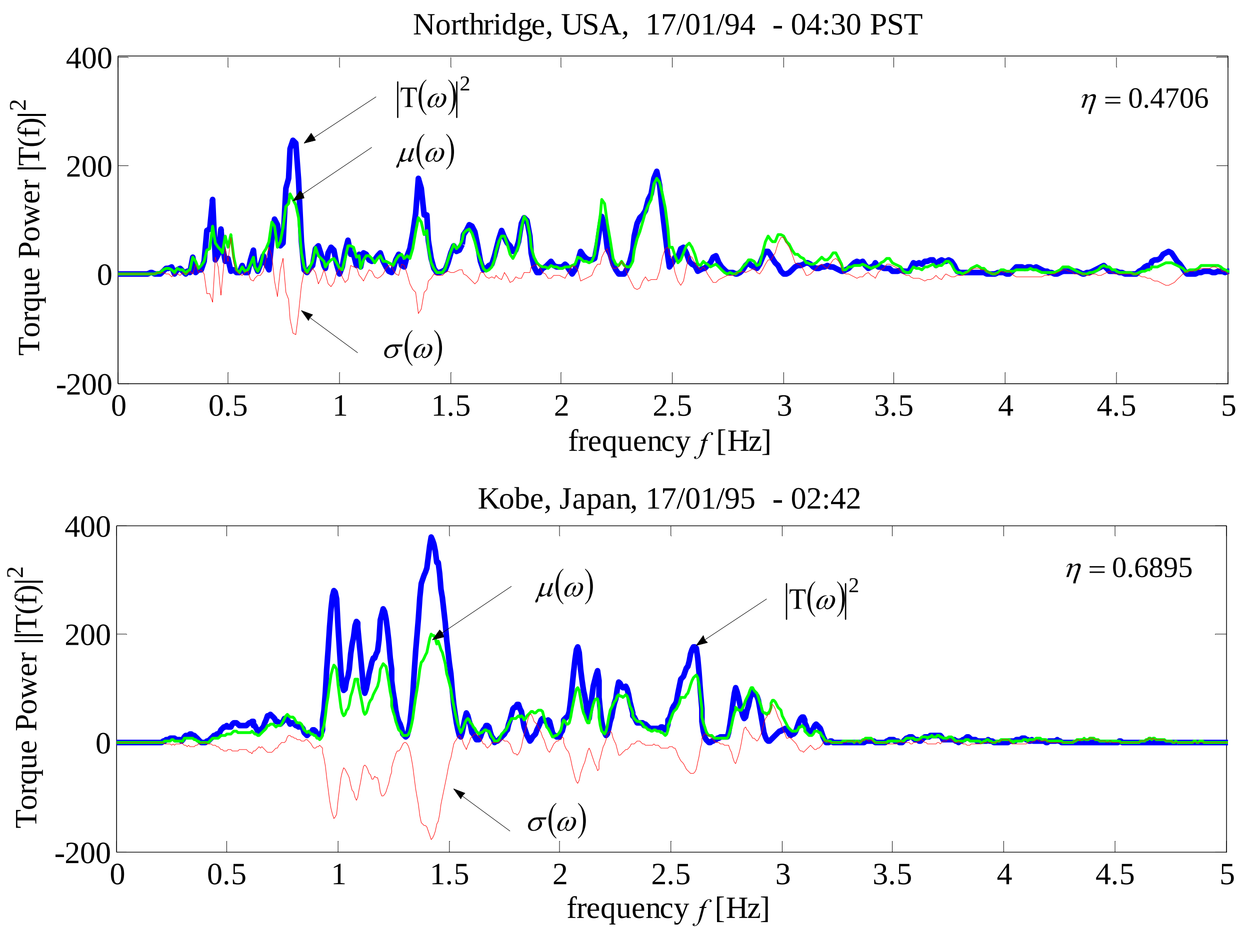

Figure 2, Comparison of two applied torque power for two events, $\varepsilon_x = \varepsilon_y = 0.1$

The conditions for the maximum of (5) are governed by $\sigma(\omega)$ and are given in equation (7). Amplitude terms $A_x(\omega), A_y(\omega)$ are positive, by definition.

$$|T(\omega)|_{\max} \text{ occurs at } \phi_D(\omega) = \begin{cases} \pi, & \varepsilon_x\varepsilon_y > 0 \\ 0, & \varepsilon_x\varepsilon_y < 0 \end{cases}, \quad |T(\omega)|_{\min} \text{ occurs at } \phi_D(\omega) = \begin{cases} 0, & \varepsilon_x\varepsilon_y > 0 \\ \pi, & \varepsilon_x\varepsilon_y < 0 \end{cases} \tag{7}$$

The relative magnitudes of terms $\mu(\omega)$ and $\sigma(\omega)$ depend on the amplitude eccentricity terms $A_x(\omega)\varepsilon_y$ and $A_y(\omega)\varepsilon_x$. If either is zero the phase tuning term $\sigma(\omega)$ is zero, i.e. phase components have no influence on the magnitude of $\mathrm{T}(\omega)$ in this case. Structures with only one axis of asymmetry [2], i.e. $\varepsilon_x = 0$ or $\varepsilon_y = 0$, will not observe the influence of phase tuning even if two orthogonal accelerograms are employed. If one of the amplitude eccentricity terms is large relative to the other then the magnitude of $\mathrm{T}(\omega)$ is governed by $\mu(\omega)$. As the amplitude eccentricity terms tend to similar values, i.e. $A_x(\omega)\varepsilon_y = A_y(\omega)\varepsilon_x$ equation (5) simplifies to

$$\left|\mathrm{T}(\omega)\right|^2 = 2\left(A_x(\omega)\varepsilon_y\right)^2\{1-\cos(\phi_D(\omega))\} \tag{8}$$

In this case the influence of phase tuning is most significant. At critical phase differences it can double the amplitude of this torque component or reduce it to zero.

Total power of applied inertial torque

The maximum and minimum magnitudes of Torque $\mathrm{T}(\omega)$, with respect to phase difference, are given as follows in equations (9) and (10). Due to the nature of (7) the equation (9) and (10) are dependant on the sign eccentricity ratio product; where $\mathrm{sgn}(x)$ is the signum function. They provide bounds to the total power of the Torque can be expressed in (11). These bounds mark the influence of the phase difference content of the orthogonal accelerogram pair.

$$\sigma^*(\omega) = 2\left(A_y(\omega)\varepsilon_x\right)\left(A_x(\omega)\varepsilon_y\right) \tag{9}$$

$$\begin{aligned} \left|\mathrm{T}(\omega)\right|^2_{\min} &= \mu(\omega) - \sigma^*(\omega).\mathrm{sgn}\left(\varepsilon_x\varepsilon_y\right) \\ \left|\mathrm{T}(\omega)\right|^2_{\max} &= \mu(\omega) + \sigma^*(\omega).\mathrm{sgn}\left(\varepsilon_x\varepsilon_y\right) \end{aligned} \tag{10}$$

$$\int_{-\infty}^{\infty}\left|\mathrm{T}(\omega)\right|^2_{\min} d\omega \le \int_{-\infty}^{\infty}\left|\mathrm{T}(\omega)\right|^2 d\omega \le \int_{-\infty}^{\infty}\left|\mathrm{T}(\omega)\right|^2_{\max} d\omega \tag{11}$$

The degree of phase tuning

This leads to an assessment of the *degree of phase tuning* η in a pair of orthogonal accelerograms, given by equation (12) and this η is property of the accelerogram pair and almost independent of the structural eccentricity ratios; only the sign of the eccentricity ratio product is important. When η equals 0 the phase difference of the accelerogram pair is such that it leads to a minimum power of the applied inertial torque. When η equals 1 the phase difference of the accelerogram pair is such that it leads to a maximum power of the applied inertial torque. The plus or minus sign is a consequence of the conditions (9) and (10) and which follow directly from (7). Without numerically evaluating ρ in equation (12), for a particular accelerogram pair, it is not possible to ascertain which condition $\varepsilon_x\varepsilon_y > 0$ or $\varepsilon_x\varepsilon_y < 0$ will result in the larger η and hence evaluate the larger applied torque from a particular accelerogram pair.

$$\eta = \frac{\int_{-\infty}^{\infty}\left|\mathrm{T}(\omega)\right|^2 d\omega - \int_{-\infty}^{\infty}\left|\mathrm{T}(\omega)\right|^2_{\min} d\omega}{\int_{-\infty}^{\infty}\left|\mathrm{T}(\omega)\right|^2_{\max} d\omega - \int_{-\infty}^{\infty}\left|\mathrm{T}(\omega)\right|^2_{\min} d\omega} = \tfrac{1}{2}\left\{1 - \mathrm{sgn}\left(\varepsilon_x\varepsilon_y\right)\frac{\int_{-\infty}^{\infty} A_x(\omega)A_y(\omega)\cos(\phi_D(\omega))d\omega}{\int_{-\infty}^{\infty} A_x(\omega)A_y(\omega)d\omega}\right\} = \tfrac{1}{2}(1 \pm \rho) \tag{12}$$

There is property about equation (12) such that the following statements (13) are also valid. The bound on larger η is such that it is always between 0.5 and 1.

Let $\eta_1 = \frac{1}{2}(1-\rho),\ \eta_2 = \frac{1}{2}(1+\rho)$ then $\eta_1 + \eta_2 = 1.$ (13)

In Figure 2, the value of η , degree of phase tuning, is given of each accelerogram pair. The Kobe earthquake has the larger η. This implies that if both records where used in a time-history study, and are scaled to comparable amplitude levels the Kobe pair would induce larger torsional inertial actions on the building. The usefulness of the η is that it is predominantly a characteristic of the ground motion not the structure, i.e. *it appears self-evident that some events produce more torque power than others.* However, it has yet to be shown that this increase in torque power, the system input, results in larger structural torsional responses, the system output.

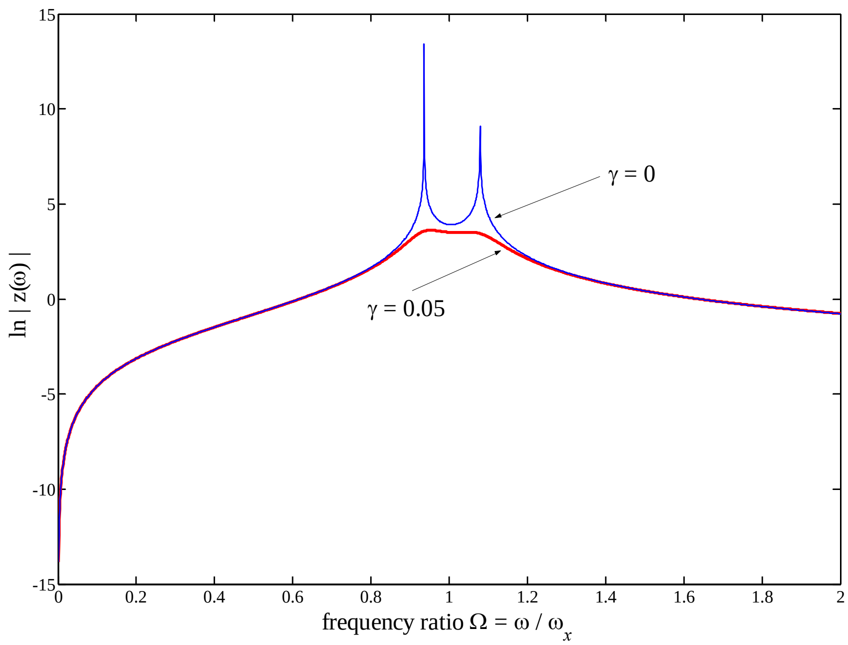

Figure 3, Torsional response transfer function: $\varepsilon_x = \varepsilon_y = 0.1$

LINEAR STRUCTURAL RESPONSE TO APPLIED INERTIAL TORQUE

By taking the Fourier transform of equation (1), the frequency domain representation of (1) is given in equation (14).

$$\underline{\ddot{u}(\omega)} = -\omega^2 \left\{ \left[\left([K] - \omega^2 [M] \right) + i \left(\omega [C] \right) \right]^{-1} \right\} \underline{\ddot{u}_g(\omega)} = [H(\omega)] \underline{\ddot{u}_g(\omega)} \qquad (14)$$

While it is, currently, feasible to evaluate this transfer matrix $[H(\omega)]$ using a computer algebra package [5]; the general, algebraic, result is dense, complex and rather un-elucidating. In order to examine some of the features of $[H(\omega)]$ a few conditions are assumed. First damping is ignored, and structural frequency parameters are assumed $\omega_x = \omega_y = \omega_\theta$; this condition should place the structure near the critical condition of coupled sway and torsional resonance. The response rotational acceleration of the structure is given by the last row of (14); thus it can be shown that the building rotational acceleration is the product of the real function $z(\omega)$ and the inertial torque $\mathrm{T}(\omega)$.

$$r\ddot{\theta}(\omega)=z(\omega)\mathrm{T}(\omega) \quad , \quad z(\omega)=\frac{\Omega^2}{\left(1-2\Omega^2+\Omega^4\left(1-\varepsilon_y^2-\varepsilon_x^2\right)\right)}, \quad \Omega=\frac{\omega}{\omega_x} \tag{15}$$

The form of this transfer function $z(\omega)$ can be visualized in Figure 3. In the more general case, when damping is present, $z(\omega)$ is a complex function given in equation (16) and its form is also displayed in Figure 3; where γ is the ratio of critical damping and damping matrix $[C]=\frac{2\gamma}{\omega_x}[K]$. In this system ω_x is an eigen-frequency.

$$z(\omega)= -((1+2i\Omega\gamma)(-1+\Omega^2-2i\Omega\gamma)\Omega^2)/(1-3\Omega^2+6i\Omega\gamma+3\Omega^4-12i\Omega^3\gamma-12\Omega^2\gamma^2-\Omega^4\varepsilon_x^2 -\Omega^6+6i\Omega^5\gamma+12\Omega^4\gamma^2+\Omega^6\varepsilon_x^2-8i\Omega^3\gamma^3-2i\Omega^5\gamma\varepsilon_x^2-\Omega^4\varepsilon_y^2+\Omega^6\varepsilon_y^2-2i\Omega^5\varepsilon_y^2\gamma) \tag{16}$$

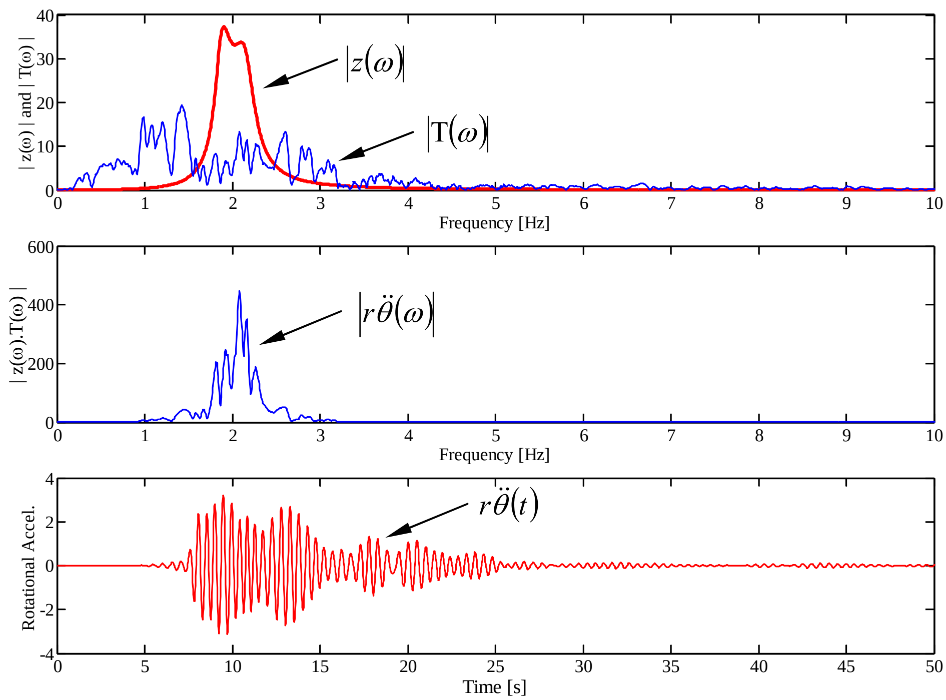

Figure 4, Kobe accelerogram pair, $\varepsilon_x=\varepsilon_y=0.1$, $\omega_x=\omega_y=\omega_\theta=4\pi$, $\gamma=0.05$

In Figure 4 an example of the frequency domain approach is visualized, torque power and torque transfer functions, top graph, are multiplied to produce torsional response power, centre graph, and time domain torsional response acceleration, bottom graph. From the time domain responses it is possible to produce torsional acceleration response spectra, shown in Figure 5. The torsional acceleration response of the Kobe event is generally larger than the Northridge event. The peak torsional accelerations are of the order of 40% larger for the Kobe event. Notice, however, at the high frequency range the Northridge spectrum exceeds the Kobe. If Figure 2 is considered, there is some torque power in this high frequency range for the Northridge event while the Kobe event has almost no power at this frequency range. Thus the influence of the degree of phase tuning on the torsional response is dependant on structural configuration.

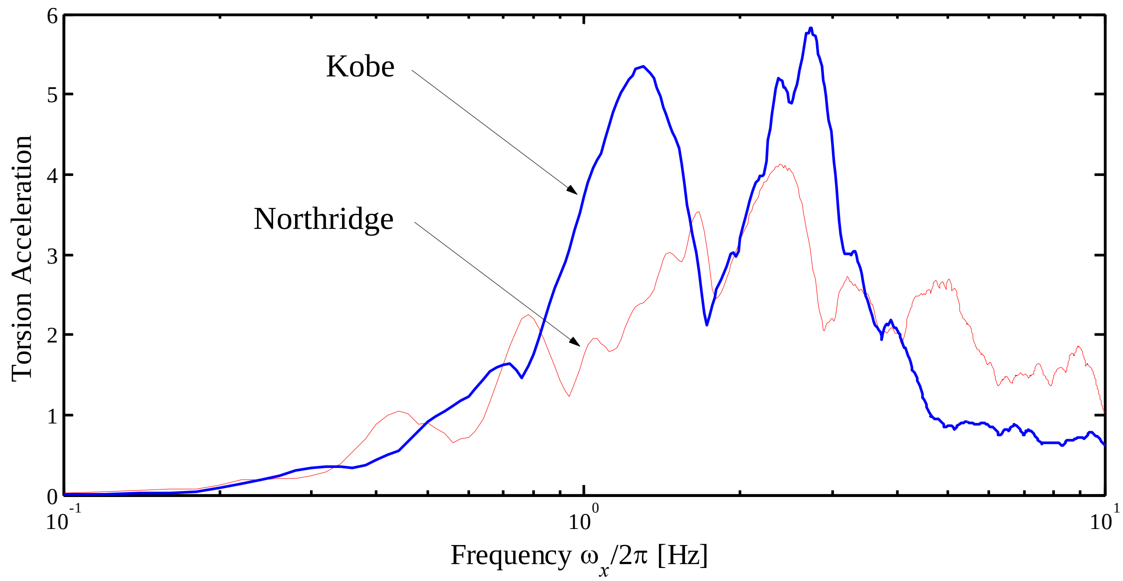

Figure 5, Torsional Acceleration Response Spectra, $\varepsilon_x = \varepsilon_y = 0.1$, $\omega_x = \omega_y = \omega_\theta$, $\gamma = 0.05$

It has now been mathematically established that the magnitude of the response torsional acceleration is influenced directly by the phase tuning term $\sigma(\omega)$ in the case of a linear structural system (1). There is an important corollary of (16); the influence of the phase tuning term is mitigated by the transfer function $z(\omega)$. The greatest influence of the phase tuning on the rotational acceleration is when frequencies at which large torque power coincide approximately with frequency band around the structural frequency parameter ω_x.

CONCLUSIONS

In this paper, analyses of asymmetric buildings subjected to seismic actions are investigated. The influence of the ground motion, amplitude and phase differences frequency components is discussed. Expressions for the frequency contents of the applied torque are proposed. Amplitude and phase difference terms are identified. The conditions for maximal torque power are explored. These maxima occur when the amplitude content at a certain frequency is large and of similar magnitude in both the x and y direction and this situation is combined with the condition of critical phase differences between these components. Under these conditions of critical phase tuning, the x and y ground motion can amplify the applied torque power by a factor of two or reduce it to zero. A concept, the degree of phase tuning between a pair of orthogonal accelerograms is introduced. This quantifies the proximity to critical phase tuning of a pair of records. The degree of phase tuning is different for different records. What is also clear is that some pairs of accelerogram records produce more applied torque power than other due to their large degree of phase tuning.
Using a classical linear frequency domain analysis, the influence of the applied torque power is mapped through the structural system's complex transfer matrix to elicit the structural response. It has been mathematically demonstrated that larger degree of phase tuning results in larger applied torque power and subsequently larger structural torsional accelerations. Linear response spectra for events presented in this paper show as much as 40% increase in peak torsional accelerations due to the phase tuning effect.

It is clear that knowledge of the amplitude-frequency content, of the ground acceleration, is necessary but not sufficient to quantify the power of the applied torque or the torsional response of asymmetric structures. Larger degrees of phase tuning generate, in nonlinear structural systems, either larger torsional accelerations or larger torsional ductility demands. Thus, when selecting a set of accelerograms for use in nonlinear timehistory studies, of asymmetric buildings, it is necessary to recognize the influence of the degree of phase tuning. Otherwise the statistical predictions from small samples of analyses may be biased and unrepresentative of the structures performance in the case of the unknown future seismic event.

REFERENCES

1 CEN European Standard. Eurocode 8: Design of structures for earthquake resistance. Part 1 General rules, seismic actions and rules for buildings. CEN PrDRAFT No. 3, May 2001. Section 3.2.3.2, pp 21

2. Chandler, A.M.,Correnza J.C. & Hutchinson G.L, 1995 Ultimate limit state Seismic Torsional provisions in Eurocode 8. *Proc. Instm Civ. Engrs Structs & Bldgs*. 110, Feb., pp 86-97

3. Hejal, R. & Chopra, A.K. 1987. Earthquake response of torsionally coupled buildings *Earthq. Engg. Research Center, Uni. of California at Berkeley* UCB/EERC-87/20

4. Arias, A 1970, A measure of Earthquake intensity R.J ed. Seismic Design for Nuclear Power Plants, MIT press, Cambridge, Massachusetts, pp 438-483.

5. Maple 7.0, May 28, 2001.Waterloo Maple Inc.

13th World Conference on Earthquake Engineering
Vancouver, B.C., Canada
August 1-6, 2004
Paper No. 401

DEVELOPMENT OF A DECISION SUPPORT SYSTEM FOR POST-EARTHQUAKE EMERGENCY MANAGEMENT USING SYNTHETIC DATA PROCESSING TECHNIQUE

Nobuoto NOJIMA[1] and Masata SUGITO[2]

SUMMARY

A decision support system for post-earthquake emergency management is developed. In post-earthquake emergency, decision makers are involved in a significant trade-off between rapidness and preciseness of important actions. To support them, related information is integrated from different sources: rapid damage assessment based on seismic monitoring system and actual damage information. Damage estimates are updated in a sequential manner based on Bayesian updating theory, providing a rational basis for adequate action policies. Several modules are being constructed for the GIS-based decision support system. This paper introduces the basic concept and prototypes of several modules.

INTRODUCTION

One of the great lessons from the 1995 Hyogoken-Nambu Earthquake, Japan, is that rapid collection and transmission of damage information is requisite for appropriate post-earthquake response and successful damage mitigation. Accumulation of confirmed information of actual damage was extremely time-consuming process, resulting in a fatal delay in initial response. Lack of effective measures for disaster information management was recognized as a common defect at various levels of organizations such as national and local governments, utility and transportation lifelines, and private sectors in Japan. Since then, many types of real-time earthquake disaster prevention and mitigation systems have been developed and put into function for post-earthquake emergency management (Noda and Meguro [1], PWRI [2], NRIFD [3]).

Figure 1 illustrates various information sources on which such systems are based (Nojima [4]). The diagram is coordinated on the horizontal axis of time and the vertical axis of direct or indirect properties of information accounting for damage. On the lower left part, strong motion observation and related damage assessment tools are located. Since acquisition and processing of information is rapid enough, disaster-hit area can be quickly outlined and real-time warning signals can be issued for emergency actions. The upper central part is a place for the new technology of remote sensing. Visual images acquired by various types of platform such as airborne remote sensing (e.g., high-definition television

[1] Associate Professor, Dept. of Civil Eng., Gifu University, Japan. Email: nojima@cive.gifu-u.ac.jp
[2] Professor, River Basin Research Institute, Gifu University, Japan. Email: sugito@cive.gifu-u.ac.jp

image, aerial photographs) and satellite remote sensing (e.g., SAR, LANDSAT, SPOT) are used for early detection of damage (Yamazaki and Matsuoka [5], Mitomi, et al. [6]). On the right side, conventional measures of information collection such as patrol, damage inspection, and related disaster information are listed. Although time-consuming, this process is undoubtedly indispensable because of uncertainty involved in early damage estimation.

Viewing the variety and each distinctive feature of different sources of information, it is easily recognized that each information source has advantage and disadvantage in terms of rapidness and accuracy in emergency response (See Figure 2). Then, new kinds of questions are posed to disaster responders. How can they bridge the gap between initial damage estimation and actual damage information considering the balance of rapidness and accuracy? How can they best utilize all kinds of information? How well can they manage emergency conditions in initial information-less period and subsequent information-inundated period?

To answer these questions, integration of gathered information and updating of estimation become key considerations. The authors are developing a GIS-based decision support system for post-earthquake emergency management based on synthetic data processing of damage information. The principle concept is to combine pre-event and/or real-time estimation of damage with observational damage information in a sequential manner using Bayesian approach, and to provide decision makers with rational basis for what to do with emergency response and when to activate the emergency measures.

This study presents a theoretical background and module development of the decision support system. First, a seismic intensity data processing module is constructed to generate initial damage estimation to be updated by the following process. Next, theoretical frameworks of a synthetic data processing module using Bayesian approach and a decision support module using the technique of SPRT (sequential probability ratio test) are presented. Finally, a prototype of decision support system for practical use is demonstrated.

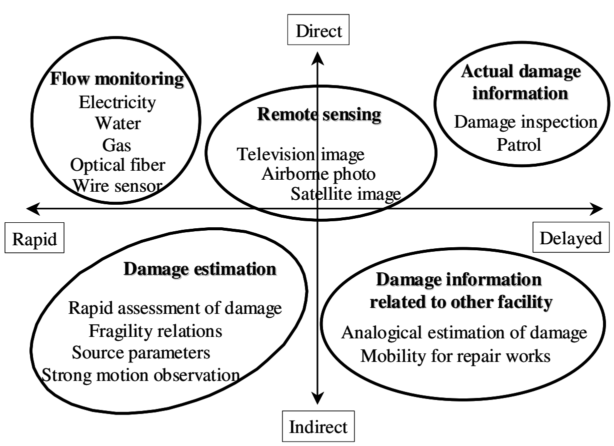

Figure 1 Various information sources in earthquake emergency response

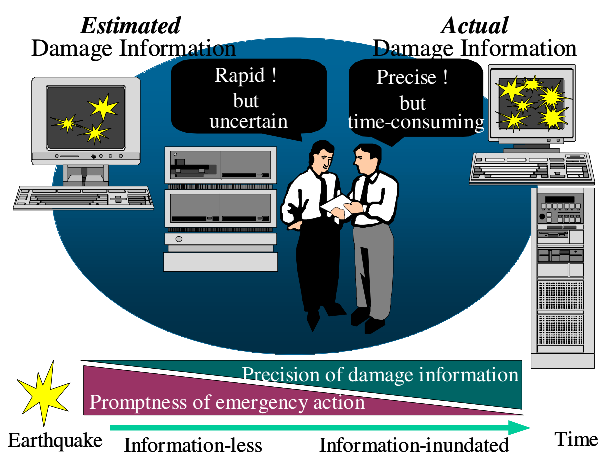

Figure 2 Rapidness and accuracy of damage information

ESTIMATION OF SEISMIC INTENSITY DISTRIBUTION

The system module for estimation of seismic intensity distribution employs a simplified method of spatial interpolation of observed seismic intensities. More emphasis is placed on rapidness rather than preciseness. Since the number of seismic observation stations is limited, interpolation is an inevitable process for estimation of seismic intensity distribution no matter how densely observatories are deployed. In this section, the module of seismic intensity estimation for Gifu Prefecture, Japan is introduced.

Receiving seismic intensity information from seismic intensity observation network

Recent development of nation-wide networks of seismometers by several governmental organizations has enhanced high-density observation of earthquake strong motions in Japan. In Gifu Prefecture, instrumentally measured JMA (Japan Meteorological Agency) seismic intensity is to be reported from 99 municipalities (as of the end of FY2002) when earthquake occurs. It is presumed that the system uses the seismic intensity information immediately after an earthquake occurs.

Estimation of seismic intensity on rock surface at each observatory

Since seismic intensity on soil surface is affected by the amplification effect of the layered ground, it is converted to that on rock surface with shear wave velocity of approximately 500-600 m/sec. To realize rapid calculation, a conversion table was prepared in advance instead of performing dynamic response analysis. The conversion table plays a role of a loop-up table representing the non-linear relationship between seismic intensity on rock surface and that on soil surface for each type of layered ground profile. In Gifu Prefecture, 49 kinds of soil profiles were modeled for earthquake damage assessment (Gifu Prefecture [7]). The entire region of the prefecture with the area of 10,600km^2 is exhaustively subdivided into 41,461 grid cells whose sizes are EW22.5” by NS15” each (approx. 500m by 500m). Each grid cell is assigned a suitable soil profile model taking account of geological and geographical condition of the site.

Interpolation of seismic intensity on rock surface

Overall seismic intensity on rock surface is obtained using spatial interpolation technique. In this study, weighted mean of seismic intensity estimated by the procedure above is adopted. Up to five observatories in the order of direct distance are selected within the range of radius of 25km from the site of interest. The reciprocal of the square of the distance was adopted as a weighting factor. In the case where an earthquake magnitude and location of hypocenter is known, residual components from the estimates based on attenuation relationship are interpolated. If seismic source information is unknown, the estimated seismic intensities themselves are interpolated. This procedure is applied to all grid cells for exhaustive estimation of seismic intensity distribution on rock surface.

Estimation of seismic intensity on surface ground

The seismic intensity at an arbitrary grid cell on rock surface is then converted to that on surface level referring the soil profile model of the grid cell of interest. The conversion table described above is used in a converse way. This procedure is applied to all grid cells for exhaustive estimation of seismic intensity distribution on surface level.

Numerical example

A numerical example is shown using a hypothetical case for an anticipated earthquake caused by rupture of the Sekigahara-Yohroh Fault (M_j = 7.7) which is located at south-west part of Gifu Prefecture. Figure 3 shows a panel representing the JMA seismic intensity information from 99 municipalities. Since this event is a hypothetical one, the values of JMA seismic intensity were calculated based on the simulated earthquake motions using the earthquake motion prediction model, EMPR (Sugito et al. [8]), and frequency-dependent equivalent linearlization technique, FDEL (Sugito [9]), for 99 representative points. Municipality-based seismic intensity is shown in Figure 4. Seismic intensity on rock surface is estimated as shown in Figure 5. In this case, although seismic source information was not used, attenuation property is clearly demonstrated. Seismic intensity distribution on the surface ground is obtained as shown in Figure 6. The contrast of seismic intensity between hard and soft ground is highlighted.

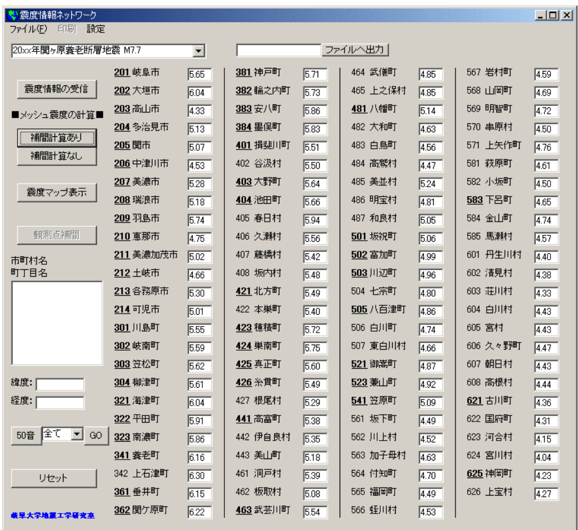

Figure 3 Seismic intensity information from 99 municipalities in Gifu prefecture

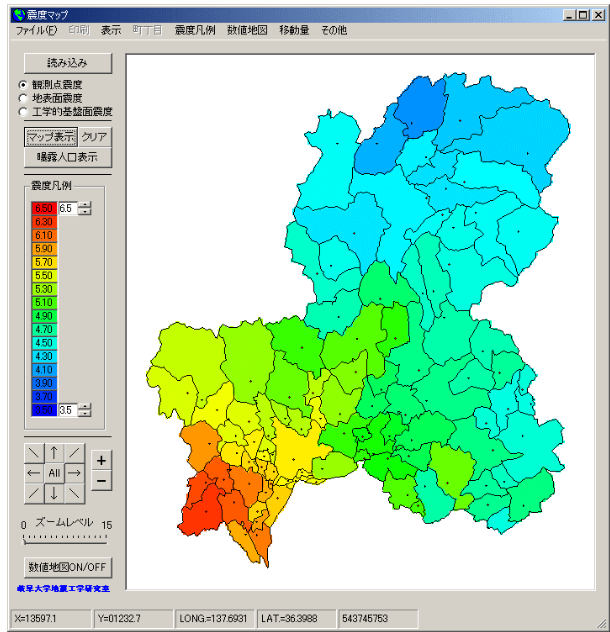

Figure 4 Seismic intensity on municipal level

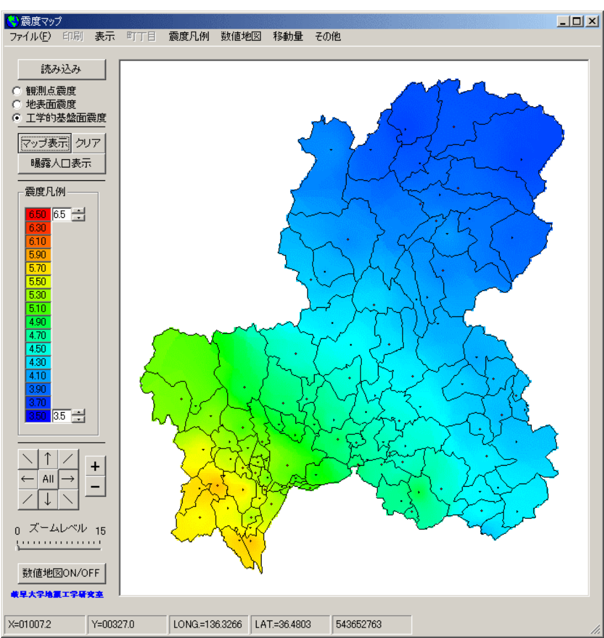

Figure 5 Seismic intensity distribution on rock surface

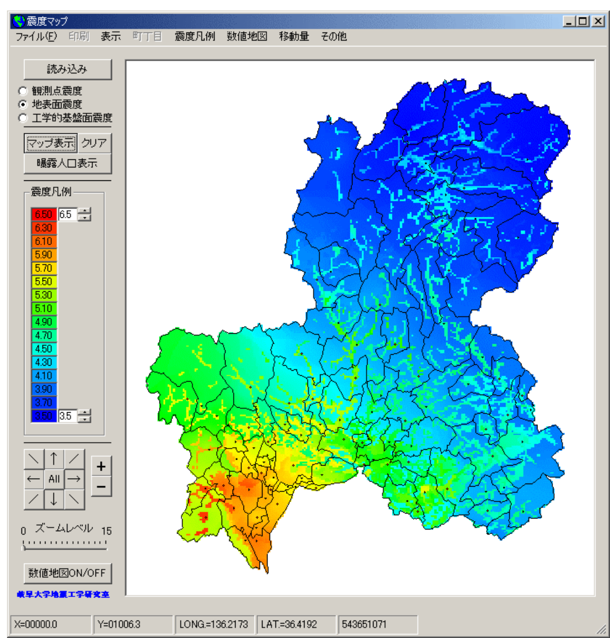

Figure 6 Seismic intensity distribution on ground surface

SEQUENTIAL UPDATE OF DAMAGE ESTIMATES BASED ON BAYESIAN APPROACH

Conventional approach and Bayesian approach

In post-earthquake damage estimation based on seismic intensity, in general, estimated values of damage probability are dealt with deterministically without consideration of uncertainty inherent to the fragility function. For example, let us consider three-fold damage ranks of wooden houses, i.e., “collapse”, “partial damage”, and “no damage”. Let p_1, p_2 and p_3 ($= 1 - p_1 - p_2$) be the estimated probabilities based on fragility function. Given the total number of houses denoted by N, the estimated numbers of structures attributed to each damage rank are deterministically represented as $N \cdot p_1$, $N \cdot p_2$ and $N \cdot p_3$, respectively. Ordinary real-time earthquake disaster prevention systems are not capable of associating initial damage estimates with subsequent actual damage information. Therefore, estimating damage is only one-time performance immediately after the earthquake, since the estimates are not updated in consideration of actual damage which are to be unveiled gradually.

In Bayesian context, on the other hand, a probability is an expression of the *degree-of-belief*. The Bayesian approach allows one to associate prior information (or engineering judgment) with observational data and it provides a formal procedure for systematic updating of information (Ang and Tang [10]). In this study, Bayesian updating procedure is adopted to incorporate actual damage information subsequent to initial damage estimation. To do this, appropriate uncertainty must be given to estimates at an arbitrary stage of investigation.

The uncertainty of initial damage estimates is represented by so-called “pre-investigation hypothetical samples.” Although both “two out of ten” and “200 out of 1000” mean the probability 0.2, statistical likelihood (degree-of-belief) of these two is obviously different. Since the denominator can be interpreted as the number of samples from the population, the larger number of denominator means higher certainty of estimated probability. Using this nature, “pre-investigation hypothetical samples” takes the form of “numbers of damage are estimated as $n_0'_1$, $n_0'_2$, and $n_0'_3$ ($= M_0' - n_0'_1 - n_0'_2$) out of the total number M_0'”.

It is presumed that the degree of uncertainty of damage estimates gradually decreases with the process of investigation. In statistical terms, investigation is considered as a process of taking samples from population in a sequential manner. The next two subsections describe the sequential damage estimation model based on Bayesian approach in terms of damage probability and number of damage, respectively (Nojima and Sugito [11]).

Sequential estimation of damage probability

Consider a group of structures of total number M_T subject to uniformly random occurrence of K-fold damage modes with probability of occurrence $\mathbf{p} = \{p_k \mid k=1, ..., K \}$. Assume that the p.d.f. of the number of damage $\mathbf{n} = \{ n_k \mid k=1,..., K\}$ can be modeled by the multinomial distribution with parameter p_k,

$$P(\mathbf{n} \mid M, \mathbf{p}) = M! \prod_{k=1}^{K} \frac{p_k^{n_k}}{n_k!} \tag{1}$$

where M denotes the total number of structures (the sum of n_k). Suppose that the number of damage is confirmed to be n_{0k} (in total M_0), as a result of investigation of damage from the partial samples M_0 ($< M_T$). Figure 7 schematically shows the situation under consideration. Since the number of damage obeys the multinomial distribution, the posterior distribution of p_k when n_{0k} damage have been confirmed is obtained as the Dirichlet distribution. Assuming the diffuse prior for the p.d.f. of p_k at the initial stage, the distribution is represented by:

$$f_p(\mathbf{p} \mid M_0, \mathbf{n_0}) = \Gamma(M_0 + K) \prod_{k=1}^{K} \frac{p_k^{n_{0k}}}{\Gamma(n_{0k} + 1)} \tag{2}$$

Introducing the “pre-investigation hypothetical samples” with a set of parameters (M_0', $n_0'{}_k$) mentioned above as the prior distribution, the posterior p.d.f. of p_k is represented by:

$$f'_p(\mathbf{p} \mid M_0, M'_0, \mathbf{n_0}, \mathbf{n_0}') = \Gamma(M_0 + M'_0 + K) \prod_{k=1}^{K} \frac{p_k^{n_{0k}+n'_{0k}}}{\Gamma(n_{0k} + n'_{0k} + 1)} \tag{3}$$

In this p.d.f., the mean and the standard deviation are derived as follows.

$$\mu'_{p_k} = \frac{n_{0k} + n'_{0k} + 1}{M_0 + M'_0 + K} \tag{4}$$

$$\sigma'_{p_k} = \sqrt{\frac{(M_0 + M'_0 - n_{0k} - n'_{0k} + K - 1)(n_{0k} + n'_{0k} + 1)}{(M_0 + M'_0 + K)^2 (M_{0k} + M'_0 + K + 1)}} \tag{5}$$

Eqs.(2) and (3) implies that both are in the same mathematical form; “pre-investigation hypothetical samples” with a set of parameters (M_0' and $n_0'{}_k$) and observational data with a set of parameters (M_0, n_{0k}) are combined together, producing posterior distribution with a new set of parameters ($M_0'+M_0$, $n_0'{}_k+n_{0k}$) which is obviously a simple sum of the previous two sets. Since multinomial distribution and Dirichlet distribution are *conjugate pairs* in the Bayesian terminology, mathematical simplification of this kind is achieved (Ang and Tang [10]).

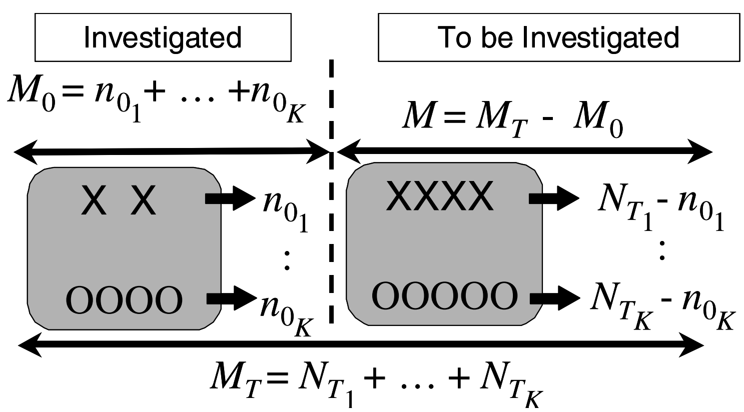

Figure 7 Schematical illustration of partial investigation

Sequential estimation of number of damage

Given the posterior distribution, the probability that damage pattern $\mathbf{n}=\{n_k \mid k=1,..., K\}$ occur for total number M can be derived as a compound distribution of Eqs.(1) and (3), producing the Dirichlet-multinomial distribution represented by the following equation.

$$P(\mathbf{n} \mid M, M_0, M'_0, \mathbf{n_0}, \mathbf{n'_0}) = \frac{\prod_{k=1}^{K} \binom{n_k + n_{0k} + n'_{0k}}{n_k}}{\binom{M + M_0 + M'_0 + K - 1}{M}} \tag{6}$$

The expected number of damage and its standard deviation for the total number M_T are derived as follows.

$$\mu'_{N_{Tk}} = n_{0k} + \mu'_{p_k}(M_T - M_0) \tag{7}$$

$$\sigma'_{N_{Tk}} = \sigma'_{p_k} \sqrt{(M_T - M_0)(M_T + M'_0 + K)} \tag{8}$$

Note that, the first term in Eq.(7), which is given deterministically, corresponds to observed number in the investigated part (in total M_0), and the second term in Eq.(7) corresponds to the updated estimate for non-investigated part (in total $M_T - M_0$) in Figure 7.

Numerical example of three-fold damage rank p.d.f.

Figure 8 shows Dirichlet distribution represented on the triangular coordinate in the cases where $M_0' = 1$, 10, and 100. In triangular axis, the red part represents relatively high likelihood, and the blue part does relatively low likelihood. The upper row shows Dirichlet distributions for $\mu_{p1} = \mu_{p2} = \mu_{p3} = 0.333$. Although peaks (modes) of those p.d.f.'s are exactly on the center of triangular coordinate, the degree of diffuseness is extremely different. When M_0'=1, the distribution is highly diffused with standard deviation of 0.211 for all damage ranks. The distribution gets narrower with increasing M_0'; the standard deviations are 0.125 and 0.045 for M_0'= 10 and 100, respectively. The lower part shows Dirichlet distributions for μ_{p1}=0.2, μ_{p2}=0.3, and μ_{p3}=0.5. When M_0'=1, the distribution is highly skewed and diffused, but with increasing value of M_0', the distribution gradually converges to the mean value.

Since the degree of uncertainty is represented by M_0', its value should be determined in consideration of preciseness of seismic intensity information and that of fragility functions. The following procedure is recommended when determining the set of "pre-investigation hypothetical samples" (M_0', $n_0'{}_k$).

1) To determine μ_{pk} on the basis of seismic intensity and fragility functions
2) To evaluate the degree of uncertainty of initial estimation of damage probability with reference to a chart such as Figure 8 and determine M_0'.
3) To determine $n_0'{}_k$ using the equation. $n_0'{}_k = \mu_{pk} (M_0'+K) - 1$.

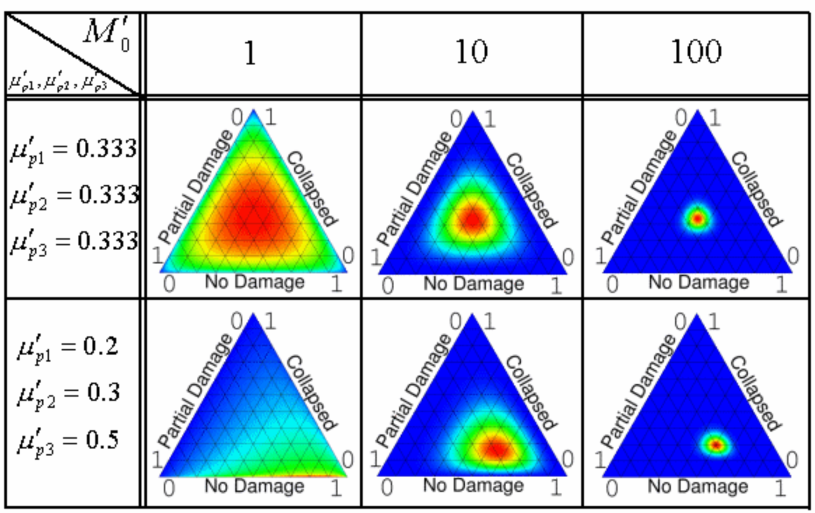

Figure 8 Dirichlet distribution with various values of M_0'

SEQUENTIAL DECISION PROCEDURE MODEL USING SEQUENTIAL PROBABILITY RATIO TEST

Upper and lower limits to activate a terminal decision

In order to determine when to make a decision under high uncertainty during the process of accumulation of damage information, the methodology of sequential probability ratio test (SPRT) developed by Wald [12] is introduced. Consider a decision rule such that an emergency measure is not activated if the damage probability of the highest rank (i.e. damage rank k=1 : collapse) does not exceed a certain limiting value p_s (null hypothesis H_0), while the emergency measure is activated if the damage rate exceeds another limiting value p_f (alternative hypothesis H_1) in which $p_s < p_f$. First of all, the likelihood ratio R_p is calculated by the following equation based on Eq.(3).

$$R_p = \left(\frac{p_f}{p_s}\right)^{n_0+n'_0}\left(\frac{1-p_f}{1-p_s}\right)^{M_0+M'_0-n_0-n'_0+K-2} \tag{9}$$

The test of statistical hypothesis lasts as long as R_p remains inside the limits of the interval represented by the following inequality (Wilks [13]).

$$\frac{\beta}{1-\alpha} < R_p < \frac{1-\beta}{\alpha} \tag{10}$$

In Eq.(10), α represents a probability (producer's risk) of an error (type I) to reject the null hypothesis H_0 even if H_0 is correct, and β represents a probability (consumer's risk) of an error (type II) to accept the null hypothesis H_0 even if H_0 is wrong. When the likelihood ratio R_p violates the lower limit, the null hypothesis H_0 is adopted, whereas the alternative hypothesis H_1 is adopted if R_p violates the upper limit. Substituting Eq.(9) into Eq.(10), the upper and lower limits for n_0 at an arbitrary stage of finishing investigation of M_0 can be written as follows.

$$\frac{(M_0+M'_0+K-2)\log\dfrac{1-p_s}{1-p_f}+\log\dfrac{\beta}{1-\alpha}}{\log\dfrac{p_f(1-p_s)}{p_s(1-p_f)}}-n'_0 < n_0 < \frac{(M_0+M'_0+K-2)\log\dfrac{1-p_s}{1-p_f}+\log\dfrac{1-\beta}{\alpha}}{\log\dfrac{p_f(1-p_s)}{p_s(1-p_f)}}-n'_0 \tag{11}$$

Effects of six parameters (p_s, p_f, α, β, M_0' and n_0') to a terminal decision

Effects of parameters p_s and p_f

These two parameters are the most important ones describing the criteria for emergency actions. The set of large values of p_s and p_f leads to detection of hardest-hit area such that $p > p_f$. On the other hand, the set of small values brings about the outline of potentially damaged area within a broad area. Therefore, these parameters must be determined cautiously taking account of such factors as the scale of disaster, conditions of damaged area, and aims of emergency actions.

Effects of parameters α and β

In Eq.(11), it can be noted that larger values of α and β give narrower interval of upper and lower bounds, resulting in rapid but erroneous terminal decisions. Conversely, smaller values of α and β give wider interval of upper and lower bounds, resulting in deliberate but delayed terminal decisions. For example, one can reach a terminal decision when the likelihood ratio becomes 1:4 in the case of $\alpha=\beta=0.20$. On the other hand, the critical ratio for terminal decision becomes 1:9 for $\alpha=\beta=0.10$, and 1:19 for $\alpha=\beta=0.05$. These facts theoretically suggest that there exists an inevitable trade-off between rapidness and deliberateness in emergency decision making.

Effects of parameters M_0' and n_0'

In Eq.(11), it can be noted that the parameters M_0' and n_0' which prescribe the prior distribution shift the upper and lower bounds downward or upward, but not the interval of the two bounds. Because of the vertical shift of boundaries, it is possible that the condition Eq.(11) is already violated before damage investigation is initiated ($M_0=0$). In such special cases, the decision maker can take action immediately after the prior distribution is obtained using, for example, real-time seismic intensity information and rapid damage assessment systems. These conditions are referred to as "real-time action criteria" herein.

NUMERICAL EXAMPLE USING A HYPOTHETICAL SEISMIC EVENTS

To demonstrate the effectiveness of the proposed system, a numerical example representing the simulation of decision making process is shown here. Simulation was performed for a hypothetical seismic event caused by the rupture of the Sekigahara-Yohroh Fault. Estimated distribution of seismic intensity for the entire Gifu Prefecture has been already shown in Figure 6. In this section, Ohgaki city is highlighted for graphical outputs. Figure 9 shows distribution of seismic intensity. Ohgaki city, which is located at southwest part of Gifu Prefecture is exposed to the intensity level ranging from 5.3 to 6.2. The method of damage estimation of wooden structure followed the one adopted by the local government of Gifu Prefecture. Wooden structures are categorized into four ranks according to the combination of construction age and type of roof; they are, in the order of seismic vulnerability, rank A (worst), rank B, rank C, and rank D (best). Fragility functions for collapse of each type of structure are shown in Figure 10.

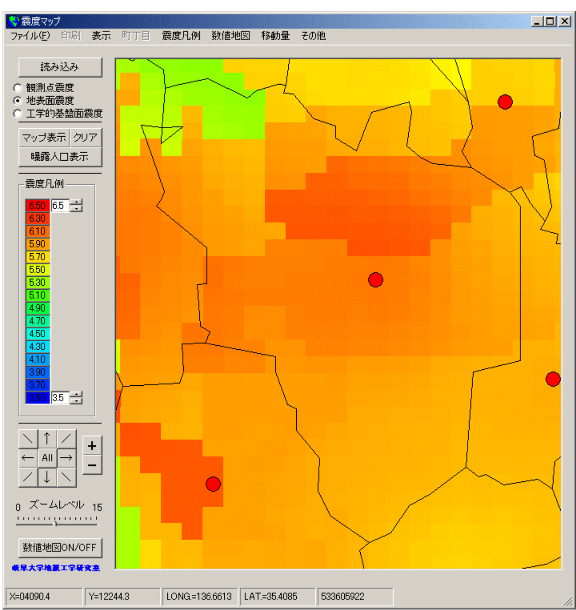

Figure 9 Seismic intensity distribution in Ohgaki city

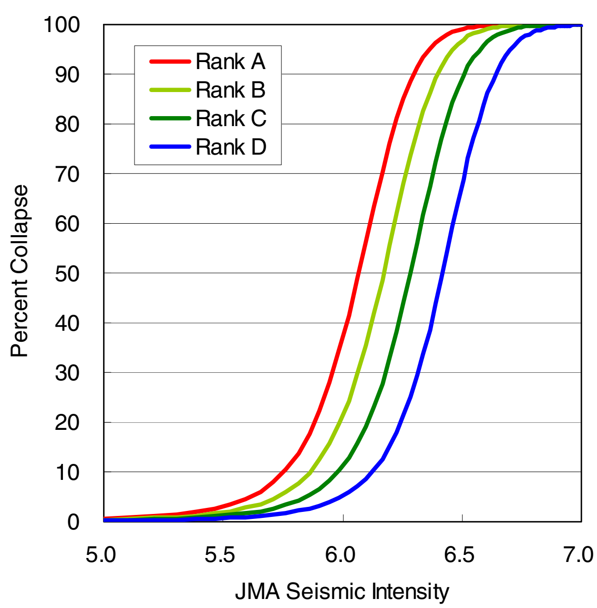

Figure 10 Fragility curves for collapse

The parameters for sequential decision process were determined as p_s =0.05, p_f =0.1, α=β=0.2, and M_0'=10. The value of n_0' was determined according to estimated values of probability of collapse and the value of M_0' above. This pattern aims at detecting heavily damaged area with more than 10% of collapsed building as soon as possible in order to take emergency actions with limited resources.

The initial status of decisions immediately after receiving seismic intensity is shown in Figure 11. Red, yellow, and blue paint correspond to activation of “emergency actions”, “decision suspended”, and “no emergency action”, respectively. Since the seismic intensity distribution shown in Figure 9 was the only information at this stage, decisions were not made in all grid cells shown in yellow. Three particular grid cells, No.1, No.2 and No.3 in Figure 11 are taken for examples herein.

The grid cell No.1 is located at the central part of the city and contains as many as 800 wooden structures. Among those, 366 buildings are rated rank A (worst) accounting for 46% of the total. Seismic intensity is estimated 6.06 and the number of collapsed houses is initially estimated as 106. The grid cell No.2 contains 250 wooden structures, and 103 of the total is rated rank D (best). Although estimated seismic intensity is 6.06, the same as No.1, initial estimate of collapsed houses is only 18. The grid cell No.3 also contains many wooden structures rated rank D (best), 63 out of the total 126. Since the estimated seismic intensity is 5.90, which is smaller than in the grid No.2, initial estimate of collapsed houses is only 3.

Next, consider the situation where damage investigation for the 10% of the total structures has been finished at a certain time after the seismic event. In this simulation, it was assumed that the real situation was consistent with the estimated one, and that the investigation was performed without bias in a spatiotemporal sense. Namely, the sequence of damage report reflected the estimated damage rate, and 10% of the total number of initial damage estimation was actually reported in each grid cell just for simplicity

Figure 12 shows the updated results. Although exhaustive investigation was not finished yet, decisions were made in 70 grid cells based on the observed information in conjunction with initial damage estimation; emergency actions taken in 18 grid cells shown in red, and no actions taken in 52 grid cells shown in blue. The grid cell No.1 is one of those where emergency actions are taken. In this cell, 11 collapsed houses were reported out of 81 houses, which means that the collapse rate was enough larger than the prescribed value of p_f. On the contrary, the grid cell No.3 is one of those without emergency actions. No collapse was reported out of 12 houses, which means that the collapse rate was enough smaller than the prescribed value of p_s. In the grid cell No.2 decision was not made at this stage yet. Although collapsed houses were few, it was judged that more investigation was needed to make a decision with required preciseness. Note that the standard deviations are significantly reduced in every case. By incorporating observation data, the degree-of-belief increases compared to the initial situation. The mean values of collapsed houses are similar to those in initial estimation because of the assumption here.

Simulations were also made for the patterns that the real situation was not consistent with the estimated one. In those sequences, the bias of initial estimates was gradually corrected as the investigation proceeded. In general, it was found that it took long time to reach final decision, when the gap between the initial estimates and actual situation is large. It was also observed that wrong decision were likely to be made when the values of α and β were set to small values. It is desirable that the initial damage estimation is made carefully with enough precision, and parameters governing the decision support system are appropriately valued.

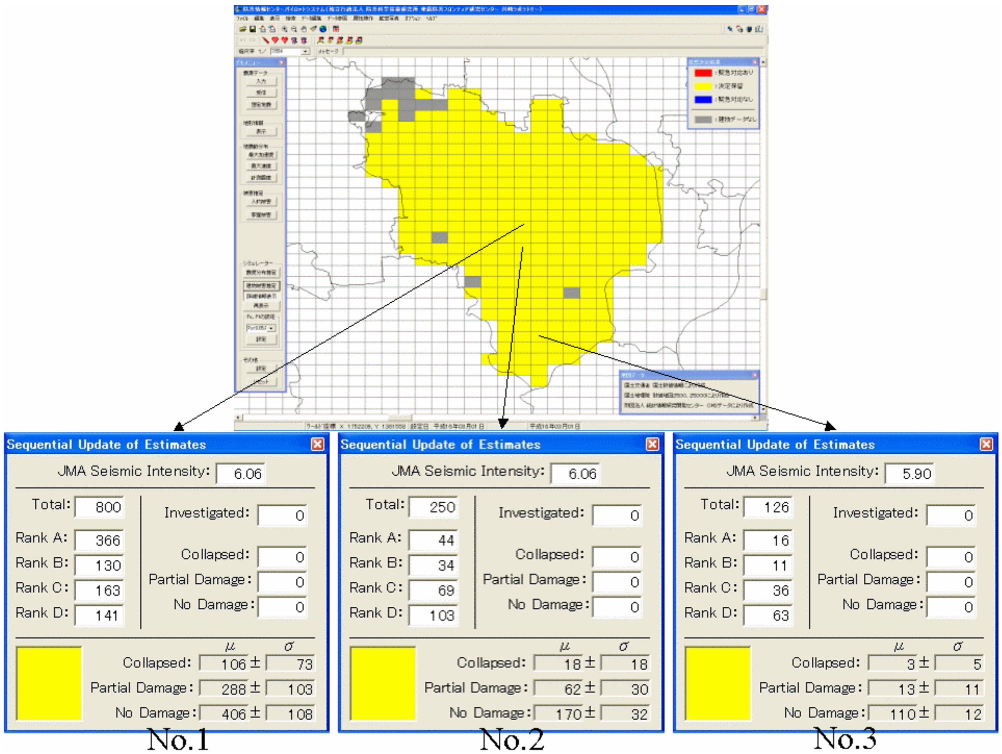

Figure 11 Result of decisions immediately after receiving seismic intensity information

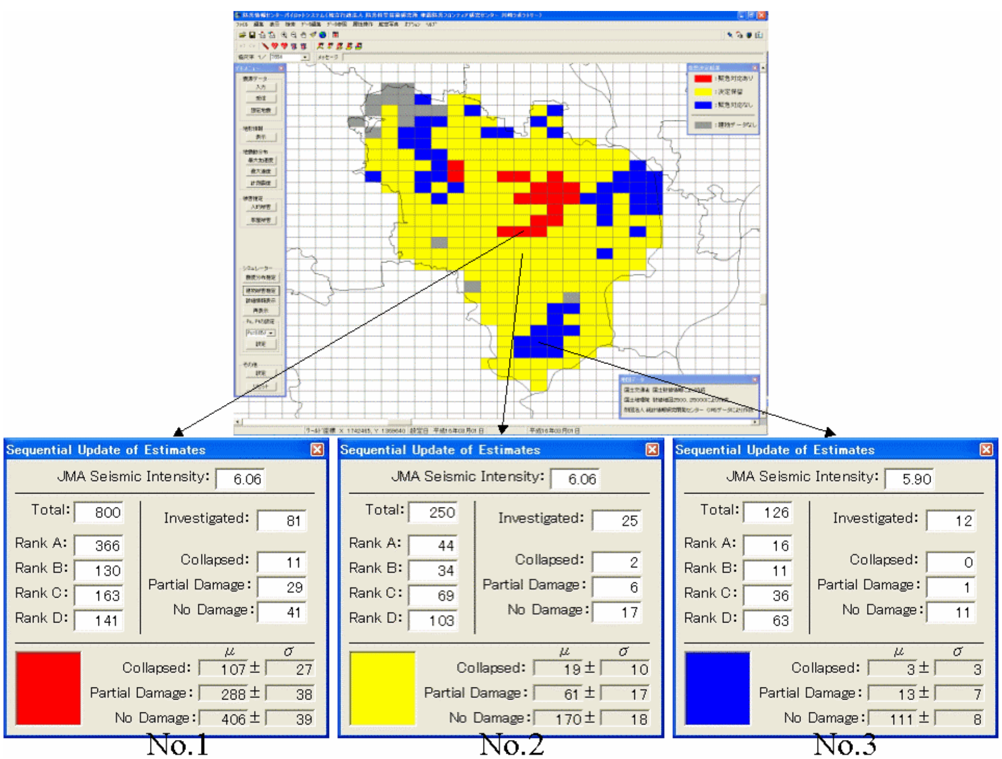

Figure 12 Result of decisions after finishing 10% investigation

CONCLUSIONS

Major conclusions derived from this study are summarized as follows.

1) A method to estimate spatial seismic intensity distribution was presented and a prototype of real-time estimation system for Gifu Prefecture was introduced. On the basis of observed seismic intensity at 99 observatories, a detailed map of seismic intensity can be obtained with 500m spatial resolutions in a real-time manner.
2) A theoretical framework for synthetic data processing of seismic damage information was presented using Bayesian approach. By combining initial damage estimation and actual damage information, damage estimates can be sequentially updated with improved accuracy.
3) A theoretical framework of statistical judgment for emergency response based on the technique of SPRT (sequential probability ratio test) was presented. Six kinds of parameters were described as important factors controlling the resultant decisions and when to make decisions.
4) As a demonstration of the effectiveness of the proposed system, a case study using the prototype of system modules was shown. Illustrated were the graphical outputs of simulation of decision making process in a hypothetical seismic event.
5) The proposed method is capable of supporting emergency responders by providing judgment criteria for emergency actions such as establishment of wide-area disaster management system, search and rescue efforts, and controlling of hazardous facility, within restrictions of time and resources.

ACKNOWEDGEMENT

This study was partly supported by the grant-in-aid for the “Special Project for Earthquake Disaster Mitigation in Urban Areas” by Ministry of Education, Culture, Sports, Science and Technology Government of Japan (MEXT). Kind assistance by Dr. Masumitsu Kuse, Collaborative Center for Academy/Industry/Government, Gifu University, Mr. Goki Hamamoto, a graduate student of Gifu University, and Mr. Takahisa Kanie, a student of Gifu University, is gratefully acknowledged.

REFERENCES

1. Noda, S. and Meguro, K. “A New Horizon for Sophisticated Real-Time Earthquake Engineering.” Journal of Natural Disaster Science, 1995, 17(2): 13-46.
2. PWRI, Ministry of Construction “Proc. of the First U.S.-Japan Workshop on Seismic Information Systems.” Tsukuba, Japan, 1999.
3. NRIFD (National Research Institute of Fire and Disaster) “Proc. of Asia-Oceania Symposium on Information Technology and Strategy for Earthquake Disaster Reduction.” Tokyo, Japan, 2002.
4. Nojima, N. “Toward the New Era of Lifeline Earthquake Engineering - After the 1995 Hyogo-ken Nanbu Earthquake, Japan -.” Proc. of the Wellington Lifelines Group International Workshop, Wellington, New Zealand, 2001: 15-20.
5. Yamazaki, F. and Matsuoka, M. “Remote Sensing: Assessing the Built Environment by Remote Sensing Technologies.” Proc. of the 2nd International Workshop on Earthquakes and Megacities, 1999: 27-34.
6. Mitomi, H., Yamazaki, F. and Matsuoka, M. “Automated Detection of Building Damage due to Recent Earthquakes using Aerial Television Images and Photographs.” Proc. of the 21st Asian Conference on Remote Sensing, 2000, Vol.1: 407-412.
7. Gifu Prefecture “A Report on Earthquake Damage Assessment in Gifu Prefecture.” 1998.

8. Sugito, M., Furumoto, Y. and Sugiyama, T. “Strong Motion Prediction on Rock Surface by Superposed Evolutionary Spectra.” Proc. of the 12th World Conference on Earthquake Engineering, Auckland, New Zealand, Paper No.2111 (on CD-ROM) 2000.
9. Sugito, “Frequency-dependent Equivalent Strain for Earthquake Response Analysis of Soft Ground.” Proc. of IS-Tokyo, The first International Conference on Earthquake Geotechnical Engineering, Tokyo, 1995: 655-660.
10. Ang, A. H-S. and Tang, W. H. “Probability Concepts in Engineering Planning and Design, Volume I - Basic Principles.” John Wiley & Sons, Inc., New York, 1975: 329-359.
11. Nojima, N. and Sugito, M. “Modeling of Post-Earthquake Emergency Decision Process Based on Data Synthesis of Seismic and Damage Information.” Journal of Structural Mechanics and Earthquake Engineering, JSCE, 724(I-62), 2003: 187-200. (in Japanese)
12. Wald, A. “Sequential Analysis.” John Weily & Sons, Inc., New York, 1947.
13. Wilks, S. S. “Mathematical Statistics.” John Weily & Sons, 1962.